Rock and Soil Mechanics 2024 45(4): 1129−1141
https: //doi.org/10.26599/RSM.2024.9435545

ISSN 1000−7598
journal homepage: rocksoilmech.whrsm.ac.cn

Present in situ stress measurement in the eastern segment of Yarlung Zangbo River fault and fault activity analysis

SUN Wei-feng[1], HUANG Huo-lin[2], SUN Dong-sheng[1], MENG Wen[1], CHEN Qun-ce[1]

1. Technology Innovation Center for In-situ Stress, Ministry of Nature Resources, Institute of Geomechanics, Chinese Academy of Geological Sciences, Beijing 100081, China; 2. PowerChina Huadong Engineering Corporation Limited, Hangzhou, Zhejiang 311122, China

Abstract: In order to determine the in situ stress state of the newly built hydropower station project in Jiacha county, and understand the activity of the eastern segment of the Yarlung Zangbo River fault zone, we obtained the in situ stress data in the engineering field by using the self-developed deep-hole stress measuring equipment based on the hydraulic fracturing method. We analyzed the fault activity by employing the Mohr-Coulomb failure criterion and the collected in situ stress data along the eastern segment of the Yarlung Zangbo River fault zone. The results showed that: (1) The magnitudes of the maximum horizontal principal stress S_H ranged from 6.07 MPa to 37.62 MPa, the values of the minimum horizontal principal stress S_h were from 3.13 MPa to 20.33 MPa at the depth from 122.75 m to 418.75 m, and the dominant direction of the measured maximum horizontal principal stress was nearly NNE. (2) The stress regime was mainly characterized by $S_H > S_h > S_v$ (S_v is the vertical principal stress), which was prone to reverse faulting. (3) Most of the measured and collected Mohr stress circles intersected the failure threshold line with friction coefficient equal to 0.6, which indicated that the eastern segment of the Yarlung Zangbo River fault zone was in a high level of fault slip instability. Furthermore, the fault slip risk of the west section from Gongga to Langxian was higher than that of the east section near Linzhi along the eastern segment of the Yarlung Zangbo River fault zone.

Keywords: in situ stress; hydraulic fracturing method; fault activity; Yarlung Zangbo River fault; Qinghai-Xizang plateau

1 Introduction

In situ stress refers to the stress present in underground rock masses. Various tectonic phenomena occurring on the surface and inside the crust, as well as accompanying geological disasters, are closely related to in situ stress, which is the primary cause of neotectonic movements such as crustal deformation, fracture, folding, and even earthquakes[1–5]. Against the backdrop of rapid economic development, China’s underground engineering construction speed ranks among the world’s fastest[6-7]. In recent years, major projects like the Sichuan–Xizang Railway, Yunnan–Xizang Railway, and large hydropower stations have been successively undertaken. Geological safety risks have become a key factor limiting underground engineering construction in the high-stress area of the Qinghai–Xizang Plateau[8–11].

The Qinghai–Xizang Plateau experiences the most intense tectonic activity globally and is the primary area of China’s western tectonic stress zone, a first-class in situ stress zone. Due to the continuous extrusion and collision of the Indian Plate in the northeast direction, the magnitude and depth-dependent gradient of the principal stress in the Qinghai–Xizang Plateau is significantly larger than in other regions [12–13]. In situ stress measurement in the hinterland of the Qinghai–Xizang Plateau began late due to its unique geographical conditions. In the early 21st century, Liao et al.[14–16] conducted systematic in situ stress measurement along the Qinghai–Xizang Railway using the piezomagnetic stress relief technique. They established in situ stress profiles from the north to the south of the hinterland and obtained shallow in situ stress data before and after the 2001 Kunlun Mountain Ms8.1 earthquake[17], providing fundamental information for researching the present tectonic stress field and earthquakes in the Qinghai–Xizang Plateau.

Since 2010, the stability and safety problems of underground caverns caused by the high in situ stress have become very prominent during the construction of projects such as the Lhasa–Rikaze Railway, Sichuan–Xizang Railway (Lhasa–Linzhi section), and Zangmu Reservoir (the largest hydropower station built in Xizang at present) along the Yarlung Zangbo River Gorge[18–19]. Now, a pumped storage power station is planned to be built in the middle and upper reaches of the Yarlung Zangbo River, south of the Qinghai–Xizang Plateau. In the vicinity of the engineering site, the state and distribution characteristics of in situ stress are obtained using the hydraulic fracturing method. With

Received: 4 May 2023 Accepted：28 September 2023
This work was supported by the Geological Survey Project of China Geology Survey (DD20242395, DD20190319)
First author: SUN Wei-feng, male, born in 1977, PhD, Senior Engineer, research interests: measurement of geostress and analysis of tectonic stress field. E-mail：sunwfcn@163.cm
Corresponding: SUN Dong-sheng, male, born in 1980, PhD, Professor, research interests: geostress measurement, structure analysis, and unconventional oil and gas. E-mail：dongshengsun@cags.ac.cn

the existing measured data of in situ stress in the eastern segment of the Yarlung Zangbo River fault zone, the fault activity is further explored, which is of great significance for the long-term operational safety of underground powerhouse in the pumped storage power station and geological safety risk assessment of surrounding projects.

2 Regional tectonic setting

Since the Cenozoic, the Himalayan orogenic belt and Qinghai–Xizang Plateau have been rising rapidly and expanding continuously under the collision and continuous convergence of Indian plate and Eurasian plate, resulting in a wide range of strong tectonic deformation on the plateau and its surrounding regions, as well as the highly complex deep processes and surface deformations[20–21]. In the Qinghai–Xizang Plateau and its surrounding regions, fault systems remarkably develop in the near east-west and north-south directions[22], and relatively parallel fault zones and linear folds are formed under this tectonic action. The Yarlung Zangbo River suture zone is located in the southern part of the Gangdisê Terrane, and its tectonic line is dominated by the NNW or NW direction. The tectonic line of the Gangdisê–Nyenchen Tangula Terrane is dominated by the NWW or EW direction, which is deflected westward near the Yarlung Zangbo River fault zone[23].

The Yarlung Zangbo River fault zone, also known as the Darjeeling–Angren–Renbu–Langxian–Medog fault zone, is located to the south of the Gangdisê–Nyenchen Tangula Mountains, and it is the boundary fault between the Gangdisê–Tengchong microcontinent and the Yarlung Zangbo River suture zone[24]. The Yarlung Zangbo River fault zone is the geotectonic boundary of the southern Qinghai–Xizang Plateau, which results from the tectonic actions of subduction–collision of the Indian Plate to the Eurasian Plate. The widths of the fracture zones in different parts of the fault zone range from hundreds of meters to more than kilometers, and obvious signs of dynamic metamorphism exist. To the west of the Darjeeling, the Yarlung Zangbo River fault zone runs north-west along the north bank of the Yarlung Zangbo River via Gongzhucuo and the southwest bank of the Kar River, and extend overseas to connect with the Indus River fault. To the east of the Darjeeling, the Yarlung Zangbo River fault zone spreads in nearly east-west direction through Angren, Lazi, Bailang, Renbu, Zedang, Jiacha, Langxian, then turns around the Great Bend of the Yarlung Zangbo River to Medog after reaching Milin, and finally extends south-east to Myanmar. The total length of the Yarlung Zangbo River fault zone is about 2 000 km. Bounded by Zhongba and Renbu, the Yarlung Zangbo River fault zone can be divided into eastern, central, and western segments, and the activities of those segments are obviously different. The more active faults in the east of Milin are Holocene active faults, while the activity of faults in the west of Milin to Zhongba is weaker, and the latest active epoch is mainly Middle-Late Pleistocene[25–26]. The Yarlung Zangbo River fault is active nowadays, dominated by right-lateral strike-slip, and its activity rate is 5.0 ± 3.0 mm/a[27]. The Yarlung Zangbo fault is dominated by thrust and belongs to the Oligocene–Miocene intense squeezed thrust deformation zone. The indications of thrust and rock deformation are particularly obvious especially near the fault in the Langxian, and there is no activity sign since the Pliocene[28].

Prior to the implementation of major projects such as the Western Transportation Project, the methods of in situ stress field investigation in the Yarlung Zangbo River fault zone were mainly qualitative or semi-quantitative evaluation methods, including inversion of focal mechanism solutions, GPS observation of crustal displacement, and numerical simulations, and a large number of studies were carried out on the direction and variation law of regional maximum principal stress. According to the earthquake catalog and the focal mechanism solution data of the Qinghai–Xizang Plateau, the seismicity in the eastern section of the Yarlung Zangbo River fault zone is dominated by small or medium shallow earthquakes, and most of the earthquakes occur at the top and the northern section of the Big Bend of the Yarlung Zangbo River[29]. The principal stress structure is characterized as reverse fault type[30–32]. From west to east, the orientation of the maximum principal compressive stress in the study area deflects from near NSE to NEE[33]. Based on the long-term GPS observation data, there is a clockwise deflection trend of the principal strain direction from west to east and from north to south[34–35]. Based on the viscoelastic upper crust model and accumulated GPS crustal displacement observation data in recent years, a large number of numerical simulations of stress–strain fields in the Qinghai–Xizang Plateau and its surrounding regions have been carried out, and the deformation rates of the widely developed north-south cracks and active faults in southern Xizang have been discussed and analyzed in depth[36–38]. In recent years, with the urgent need of western engineering construction, the in situ stress measurement has been carried out in the key sections of engineering construction, especially in the Yarlung Zangbo River Gorge, and a certain amount of in situ stress measurement data has accumulated[39–43]. The measured data show that the maximum horizontal principal stresses range from 2.01 MPa to 30.30 MPa and the minimum horizontal principal stresses range from 1.40

MPa to 16.69 MPa within the measurement depth from 40.0 m to 600.0 m. The gradients of the maximum and minimum horizontal principal stresses with the increase of the depth are 40.8 MPa/km and 25.6 MPa/km. The principal stress structure is dominated by reverse faults and strike-slip faults, and the direction of the maximum principal stress is NNE.

3 In situ stress measurement through ZKJ01 hole by hydraulic fracturing method

3.1 Overview of hydraulic fracturing

The hydraulic fracturing is an effective method to measure the stress state of rock masses deep in the crust, and it has been widely used in engineering practice. The hydraulic fracturing method is one of the methods recommended by the International Society for Rock Mechanics (ISRM)[44], and it is a method that enables direct stress measurements in deep holes. By the hydraulic fracturing method, the present in situ stress data can be obtained without the mechanical parameters of the rock. The method has the characteristics of easy operation, continuous or repeated testing at different depths, no theoretical measurement depth limit, quick measurement, and high data reliability[46–47]. Therefore, the method has been widely used in the fields of hydropower and transportation engineering as well as seismic and geological research in recent years, and a large number of in situ stress measurements have been achieved[48–50].

3.2 Measurement principle of hydraulic fracturing

The conventional in-situ stress measurement using the hydraulic fracturing method is founded on elastic mechanics. It assumes that: (i) the rock mass in the test section is linear-elastic, homogeneous, and isotropic; (ii) the rock mass in the test section is intact and devoid of natural fissures; (iii) one principal stress direction is parallel to the borehole axis; (iv) the failure of the rock mass in the test section aligns with the first strength theory (the theory of maximum tensile stress).

When the pressure is vertically applied to the hole wall, the stress state can be simplified as plane strain. The stress state around the hole can be determined using the infinite plate problem, where two principal stresses act on a circular hole with a radius of a (Fig. 1) and a homogeneous liquid pressure of P_m exists in the circular hole. A local coordinate system $X'Y'$ is established around the borehole (the axes are parallel to σ_1 and σ_2), and the stress function around the borehole can be obtained using the classical Kirsch solution[51]. The natural coordinate system XY is established (X-axis is along the east direction, and Y-axis is along the north direction), and the rock failure criterion during hydraulic fracturing follows the first strength theory. This means that the tensile fracture occurs along the direction of the minimum principal stress, and the crack direction aligns with the direction of the maximum principal stress. The fracture direction forms an angle of a with the X-axis ($\sigma_1 > \sigma_2$ and the permeability of the surrounding rock is 0).

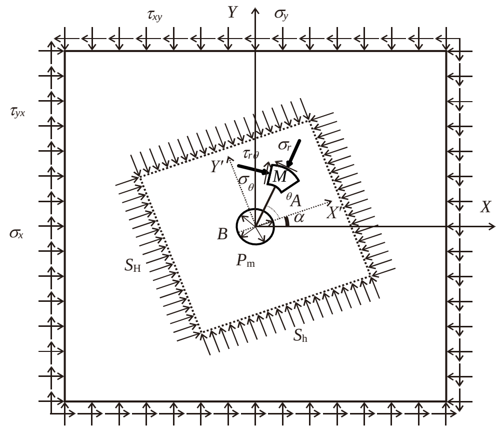

Fig.1 Stress distribution around vertical borehole with high inner pressure[52–53]

$$\sigma_r = \frac{S_H + S_h}{2}\left(1 - \frac{a^2}{r^2}\right) + \frac{S_H - S_h}{2}\left(1 - \frac{4a^2}{r^2} + \frac{3a^4}{r^4}\right) \cdot \cos(2\theta) + P_m \frac{a^2}{r^2} \tag{1}$$

$$\sigma_\theta = \frac{S_H + S_h}{2}\left(1 + \frac{a^2}{r^2}\right) - \frac{S_H - S_h}{2}\left(1 + \frac{3a^4}{r^4}\right) \cdot \cos(2\theta) - P_m \frac{a^2}{r^2} \tag{2}$$

$$\tau_{r\theta} = \frac{S_H + S_h}{2}\left(1 + \frac{2a^2}{r^2} - \frac{3a^4}{r^4}\right)\sin(2\theta) \tag{3}$$

where σ_r is the radial stress, σ_θ is the tangential stress, $\tau_{r\theta}$ is the shear stress, P_m is the pressure inside the borehole, r is the distance from point M to the center of the circular hole, θ is the angle between point M and the maximum principal stress σ_1, S_H is the maximum horizontal principal stress, S_h is the minimum horizontal principal stress (when drilling a vertical hole, σ_1 can be considered as S_H, and σ_2 can be considered as S_h). The tangential stresses generated at the two points of the borehole wall A and B (fracture point) are

$$\sigma_A = \sigma_B = 3S_h + S_H + P_m \tag{4}$$

When the pressure P_m inside the borehole reaches the fracture pressure P_b of the surrounding rock and the re-opening pressure P_r, the following equations apply:

$$3S_{\mathrm{h}} - S_{\mathrm{H}} + P_{\mathrm{b}} = T \quad (5)$$

$$3S_{\mathrm{h}} - S_{\mathrm{H}} + P_{\mathrm{r}} = 0 \quad (6)$$

$$S_{\mathrm{h}} = P_{\mathrm{s}} \quad (7)$$

$$S_{\mathrm{v}} = \sum_{i=1}^{n} \gamma_i \cdot D_i \quad (8)$$

where P_{s} is the closing pressure, T is the tensile strength of the rock mass, γ_i represents the density of the i^{th} stratum and D_i represents the thickness of the i^{th} stratum. According to the above parameters, the horizontal principal stresses S_{H} and S_{h} on the cross-section of the borehole can be determined. The vertical principal stress S_{v} can be calculated using Eq.(8).

3.3 Measurement device and process

The hydraulic fracturing measurement system includes high-pressure pump, pressure control system, data processing system, and downhole measurement device (Fig. 2), and the core of the downhole fracturing device consists of a push-pull valve, a pair of straddle expandable packers, and fracturing sections. During the field measurement using the hydraulic fracturing method, the fracturing test is first carried out after selecting the complete core section. The downhole device is placed in the measurement section using a drill rod, and a pair of expandable packers are used to seal off a section of the borehole at the selected measurement depth. Then the test section (often referred to as the fracturing section) is pressurized by pumping in fluids, and the changes of pressure and flow rate with time are recorded using the digital acquisition system (Fig.3). Based on the measured pressure−time and flow rate−time curves, the characteristic pressure parameters are obtained by analyzing the response process of borehole pressure injection and induced fracturing. According to Eqs. (5) to (7), the maximum and minimum horizontal principal stresses at the measurement points as well as mechanical parameters of the rock such as the tensile strength can be determined[45].

The fracturing measurements can be followed by the determination of the induced fracture orientation, so that the direction of the maximum horizontal principal compressive stress can be ascertained. The commonly used method is the impression orientation method, which directly records the induced fracture traces on the borehole wall. The impression orientation system comprises an automatic direction finder and an imprinter. The imprinter closely resembles the packer in appearance, except for being covered with a layer of semi-vulcanized rubber. The direction finder is made up of a copper shell and a built-in electromagnetic compass. At the predetermined time, the electromagnetic compass records the orientation of the imprinter baseline, and the direction of the induced crack (the direction of the maximum horizontal principal compressive stress) is calculated according to the relationship between the recorded azimuth angle of the baseline and the imprint.

3.4 In situ stress measurement results of ZKJ01 hole

The ZKJ01 borehole is situated on the left bank of the Yarlung Zangbo River in Jiacha County, Shannan City, Xizang Autonomous Region, at an elevation of 3,640 m. The lithology of the stratum exposed in the borehole mainly consists of granite, with an intact and hard core. However, the cores within the depths of 188–195 m, 257–262 m, and 320–250 m exhibit relative breakage. The borehole has a final diameter of 76 mm, a static water level of 105 m, and a total depth of 430.50 m.

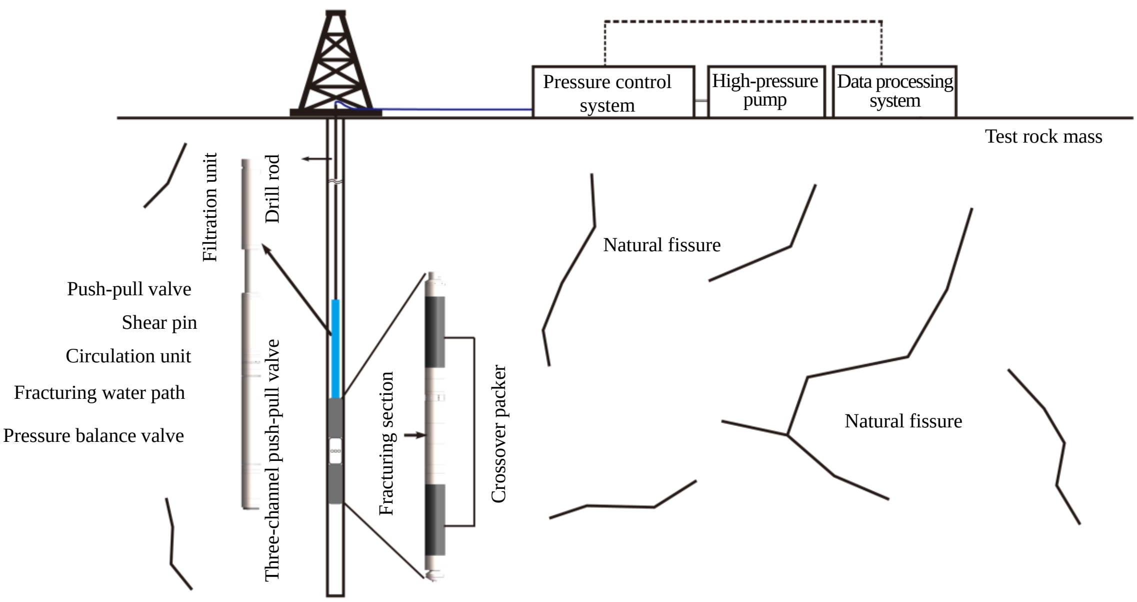

Fig.2 Sketch of the hydraulic fracturing experimental setup

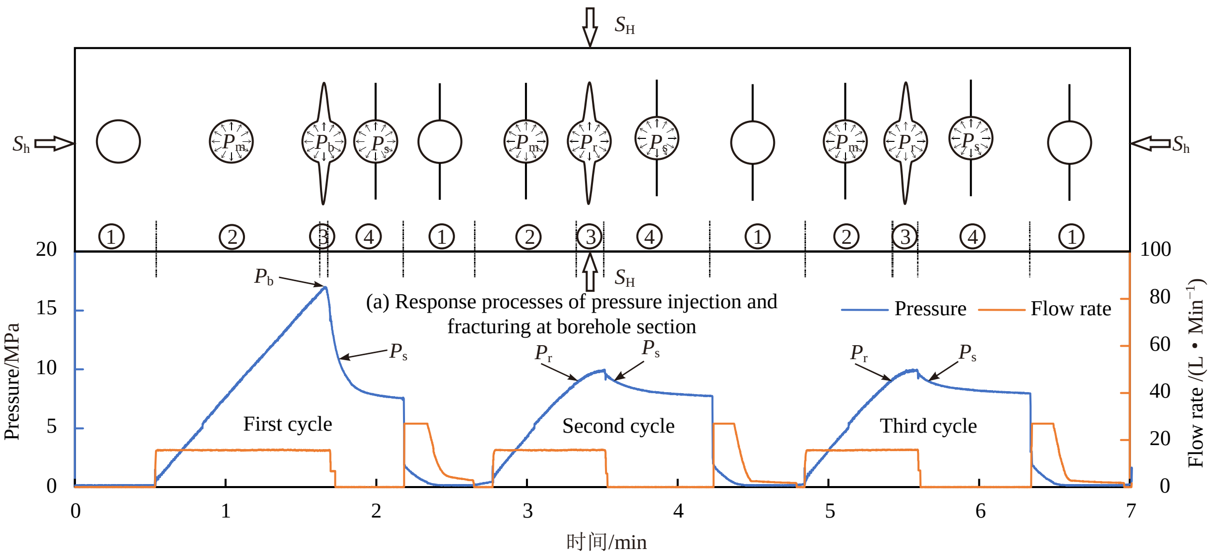

(b) Typical pressure−time and flow rate−time curves

Fig.3 Procedure of hydraulic fracturing and typical pressure−time and flow−time records[54]

The measurements were carried out using our self-developed deep-hole measuring equipment (Fig. 2). Twelve depth segments were selected for in situ stress measurement based on engineering design requirements and core conditions, with a maximum measurement depth of 418.75 m. The typical fracturing curves are shown in Fig. 4, revealing evident fracture pressures in these measurement segments. The curves exhibit a relatively standard morphology, with distinct pressure points corresponding to the opening and closing of the fractures, which can be utilized to determine the relevant pressure parameters.

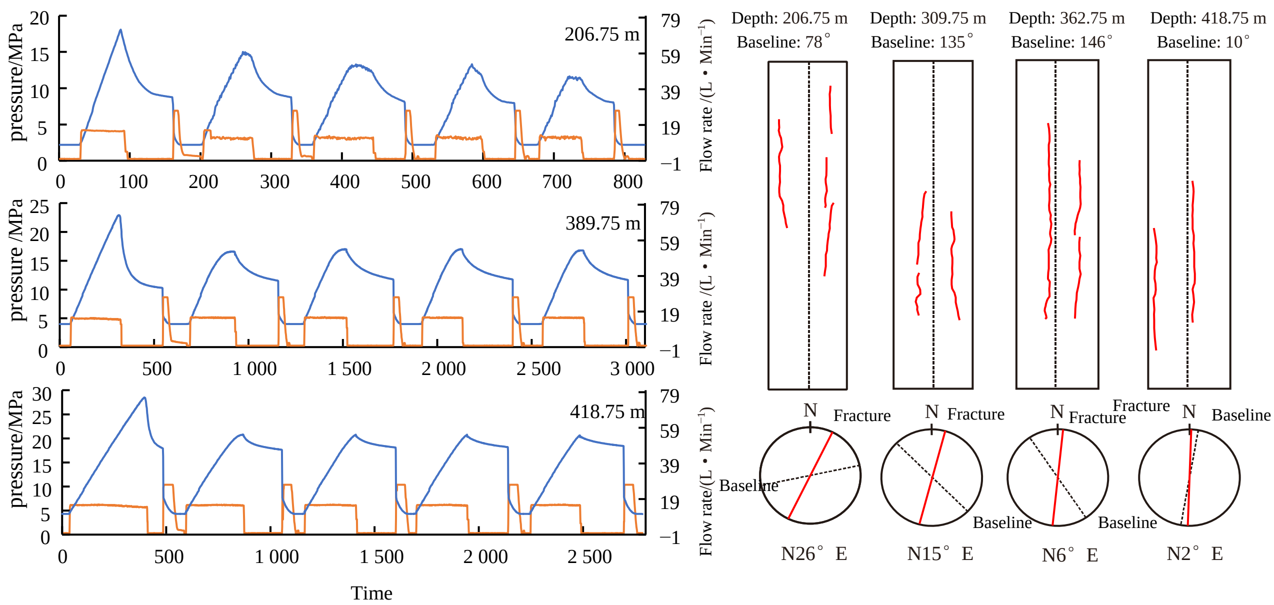

(a) Fracturing curves (b) Impression test results

Fig.4 Typical pressure−time records and impressed results of borehole ZKJ01

The fracture pressure P_b, re-opening pressure P_r, and closing pressure P_s of each measurement segment are determined according to the characteristics of the fracturing curve of each segment,. Various calculation methods, including the tangent method, such as tangent method, dt/dP method, dP/dt method, and Muskat method[55–56] are available for calculating the closing pressure P_s .The ISRM recommends using at least two or more calculation methods[45]. The self-developed computer software was used to assist in determining the characteristic pressures of fracturing curves (Fig. 5(a)), so as to calculate the maximum horizontal principal stress and the minimum horizontal principal stress of each measurement section. The vertical principal stress was estimated based on the weight of the overlying rock layer, with a rock density of 2.70 g/cm^3.

3.5 Analysis of test results

3.5.1 Measured in situ stress

The variation of in situ stress with depth partially reflects the stress state of the upper crust. Analyzing in situ stress measurement data is a crucial method for studying regional stress field characteristics. In the ZKJ01 borehole, hydraulic fracturing was used for in situ stress measurements (refer to Table 1 and Fig. 5). The maximum horizontal principal stress ranges from 6.07 MPa to 37.62 MPa, while the minimum horizontal principal stress ranges from 3.13 MPa to 20.33 MPa within the measured depth range. Notably, the horizontal principal stress between 300 and 354 m depth is significantly lower, contrary to the expected depth-related increase (see Fig. 5.(b)). The rock quality designation(RQD) of ZKJ01 borehole shows substantial variations between 29.17% and 98.44% at depths of 300–354 m (refer to Fig. 5 (c)). Cores at these depths exhibit numerous low-angle oblique joints or fractured segments (see Fig.6), leading to notable reductions in horizontal principal stresses in this section (approximately half of the values measured at nearby depths).

Discontinuous structural surfaces such as joints and faults are commonly found in the Earth's crust, exerting a significant impact on the local in situ stress field[57–58]. In rock fracture zones with shallow burial depths, the rock mass typically exhibits low frictional strength, leading to areas where the local principal stress is notably diminished[59]. Consequently, during the analysis of the regional in situ stress distribution law, anomalous stress data showing strong dispersion were excluded.

Table 1 Results of in situ stress measurement for borehole ZKJ01

Number	Depth of measurement section center/m	Fracturing parameters/MPa						Principal stress/MPa			Direction of S_H
		P_H	P_0	P_b'	P_r'	P_s'	T	S_H	S_h	S_v	
1	122.75	1.23	0.18	9.58	1.91	1.90	7.67	6.07	3.13	3.31	—
2	206.75	2.07	1.02	16.25	10.37	9.12	5.88	20.11	11.19	5.58	N26°E
3	300.75	3.01	1.96	4.64	2.75	2.60	1.89	9.11	5.61	8.12	—
4	309.75	3.10	2.05	4.03	3.24	3.12	0.79	10.27	6.22	8.36	N15°E
5	343.75	3.44	2.39	3.75	2.71	2.60	1.04	9.58	6.04	9.28	—
6	354.75	3.55	2.50	8.30	3.77	4.10	4.53	13.13	7.65	9.58	—
7	362.75	3.63	2.58	19.12	12.13	11.75	6.99	27.80	15.38	9.79	N6°E
8	389.75	3.90	2.85	19.58	9.03	8.77	10.55	22.23	12.67	10.52	—
9	396.75	3.97	2.92	16.99	9.34	9.13	7.65	23.07	13.10	10.71	—
10	403.75	4.04	2.99	18.37	12.65	12.71	5.72	30.57	16.75	10.90	—
11	410.75	4.11	3.06	23.76	15.10	15.40	8.66	36.26	19.51	11.09	—
12	418.75	4.19	3.14	24.42	16.04	16.14	8.38	37.62	20.33	11.31	N2°E

Note: P_b' is the fracture pressure recorded on the ground, P_r' is the re-opening pressure recorded on the ground, P_s' is the instantaneous closing pressure recorded on the ground, P_H is the static water column pressure, P_0 is the pore pressure, T is the in-situ tensile strength of the rock mass, S_H is the maximum horizontal principal stress, S_h is the minimum horizontal principal stress, S_v is the vertical principal stress calculated based on the buried depth of the overlying rock, and the unit weight of rock is taken as 27.0 kN/m^3.

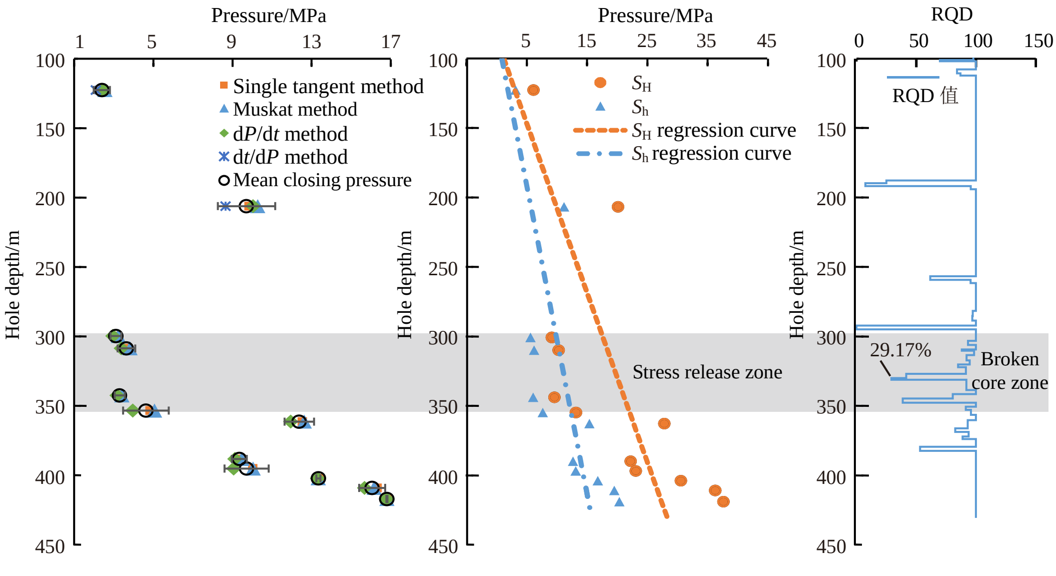

(a) Closing pressure (b) Horizontal principal stress (c) RQD value

Fig.5 Variations of horizontal principal stresses and RQD with depth for borehole ZKJ01

Generally, the principal stress in the ZKJ01 borehole increases gradually with depth, predominantly influenced by horizontal principal stress. Within the local stress anomaly zone (300–354 m), the three principal stresses exhibit the sequence S_H>S_v>S_h, creating a stress structure conducive to the formation and movement of strike-slip faults. At other depths, the principal stresses follow S_H>S_h>S_v, favoring the development and activity of reverse faults.

The core cataloging data of ZKJ01 hole show that there are pie-shaped cores at the depths of 322.9–329.7 and 401.2–401.8 m (Fig. 6). According to the previous investigation data of Zangmu Hydropower Station, there are pie-shaped core phenomena in the investigation holes such as 2# flat cave. In the exit section of Sangzhuling Tunnel in Lalin section of Sichuan-Xizang Railway, deformations of steel arches and pipe shed support, spalling of rock around the tunnel, and wall caving have also occurred [40], indicating that the study area is in high in situ stress state, which is in agreement with the results of the present in situ stress measurement.

3.5.2 In situ stress direction

Determining the direction of the maximum horizontal principal stress is based on the *Specification of hydraulic fracturing and overcoring method for in-situ stress measurement* (DB/T 14-2018)[44]. An artificially induced crack is pressurized to reopen for 20–40 minutes, resulting in a plastic bulge trace on the packer surface that aligns with the crack, indicating the direction of the maximum horizontal principal stress. From the test results of ZKJ01 hole, four representative fracturing segments underwent impression testing (Fig. 7). In the depth range of 206.75–418.75 m, the dominant direction of the measured maximum horizontal principal stress is distributed within N2°–26° E (the average is N12.25° E), indicating a dominant orientation of NNE (Fig. 7), which is largely in line with the regional principal stress direction.

(a) 322.9－329.7 m (b) 341.9－347.2 m

Fig.6 Core discing and crushed zone for borehole ZKJ01

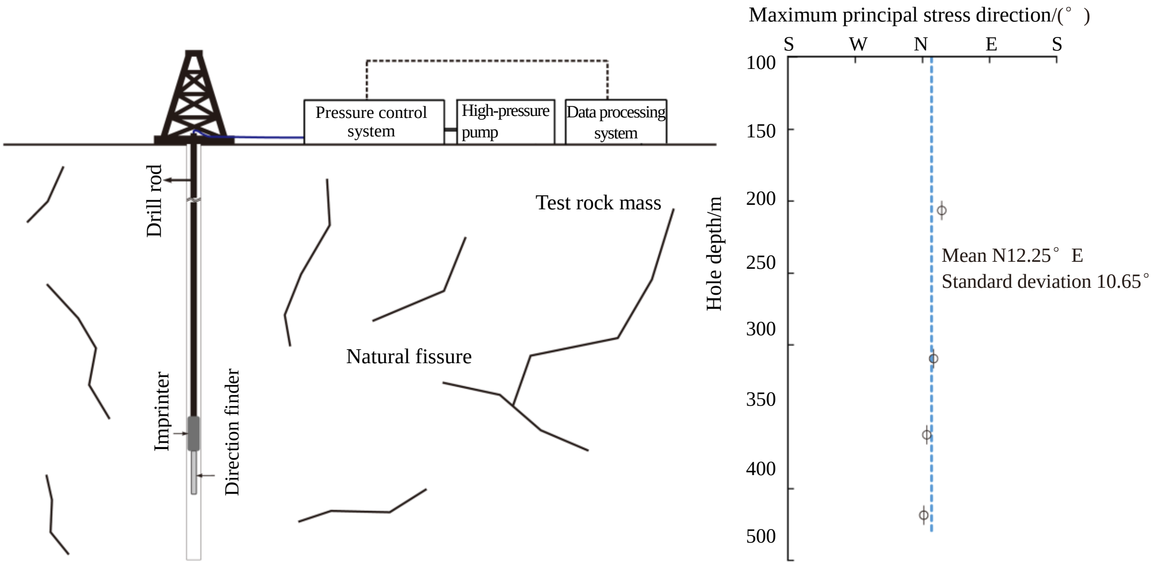

(a) In situ stress impression system for hydraulic fracturing (b) Distribution of maximum principal stress direction

Fig.7 Impression packer test setup and variation of maximum horizontal principal stress with depth for borehole ZKJ01

The current tectonic deformation of the Qinghai–Xizang Plateau is primarily characterized by north-south extrusion. The regional stress distribution is notably influenced by faults, leading to stress concentration near plate suture zones and regional faults. The north-south stress varies significantly along the fault line. Due to the strong subduction and thrusting effect of the Indian plate in the northeast direction, the motion characteristics of the current crust in the Qinghai–Xizang Plateau are dominated by east-west stretching, eastward movement, north-south extrusion, and vertical uplift. East-west shortening within the crust is mainly attributed to material outflow and clockwise rotational motion around the eastern tectonic knob of the Himalayas, while north-south shortening is primarily due to crustal thickening. In recent times, most major seismic activities in the study area have occurred along north-south strike-slip fault zones, with horizontal crustal motion direction being northeast. The modern tectonic stress field is expected to exhibit a corresponding northeastward compression, consistent with the displacement vectors derived from GPS observations in mainland China. The distribution characteristics of the tectonic stress field in mainland China were elucidated through focal mechanism solutions, fault sliding, and in-situ stress measurements. From the collision boundary between the Indian plate and the mainland China plate to the northern part of the Qinghai–Xizang Plateau, the stress field shows a clockwise rotational tendency from north-south to northeast. The current measurement site is situated in the southern part of the Qinghai–Xizang Plateau. Based on the impression test results, the maximum horizontal principal stress direction within the depth range of 206.75–418.75 m is close to NNE, aligning well with the regional stress field characteristics.

4 Discussion on the activity of the eastern section of the Yarlung Zangbo River fault zone

The ZKJ01 borehole is situated in the eastern section of the Yarlung Zangbo River fault zone in the southern Qinghai–Xizang Plateau. The east-west fractures in this area are predominantly large-scale and deep, often appearing as strike-slip or reverse thrust faults. Conversely, the north-south fractures are generally smaller in scale, forming a concentrated belt distribution. Towards the northern end of the borehole, the Yarlung Zangbo River fault zone traverses from west to east, exhibiting high seismic activity. The activity within this fault zone holds significant importance for the design, construction, and long-term operational safety of the underground plant for the pumped storage hydropower station.

The fracture processes within the Earth’s crust are highly intricate. Most fractures (faults) form and become active due to sliding damage caused by escalating shear stresses[4, 62–63]. According to the Coulomb criterion, when the shear stresses acting on the fault surface exceed or equal the frictional resistance, the fault slips. The Coulomb failure function can be mathematically represented as

$$\mathrm{CFF}=\tau-\mu\sigma_{\mathrm{n}} \tag{9}$$

where CFF is the critical friction function; τ is the fault surface friction; μ is the fault surface friction coefficient; σ_{n} is the normal stress on the fault surface. When the Coulomb failure function is negative, the fault surface remains stable and the shear stress is not enough to overcome the sliding resistance. When the Coulomb failure function is 0, the shear stress on the fault surface overcomes the resistance, leading to fault sliding. The Coulomb criterion disregards cohesion on the fault surface. Additionally, the impact of pore pressure P_0 is taken into account.

$$\mu=\tau/(\sigma_{\mathrm{n}}-P_0) \tag{10}$$

Byerlee summarized laboratory friction test data from various rocks[64] and concluded that the friction coefficient remains within a narrow range for normal stress values below 100 MPa, with μ typically ranging between 0.6 and 1.0[65–66]. The critical values for fault sliding are μ=0.6 and μ=1.0. Mohr circles were constructed using stress values measured from the ZKJ01 hole to assess fault stability in the study area (depicted by the green semicircle in Fig.8). The results indicate that most Mohr stress circles from the measured holes intersect the failure threshold for μ=0.6, suggesting a risk of sliding instability near the measurement points. Deeper measurement points (exceeding 403 m in depth) show Mohr stress circles nearing the upper limit (failure threshold for μ=1.0), indicating a higher risk of sliding instability in the vicinity of these points.

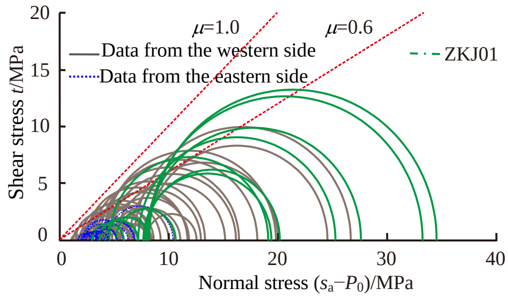

Fig.8 Mohr circles for fault stability analysis based on in situ stress data

To further investigate the stress state of the Yarlung Zangbo River fault zone, we collected data from 62 segments across 8 boreholes spanning from Shigatse to Linzhi along the fault zone (Table 2). Utilizing this data, we generated Mohr stress circles (Fig. 8). With regards to each segment’s data, most Mohr stress circles intersect the critical failure line for μ=0.6, indicating a risk of sliding instability in the regional faults, except for specific data from the ZKJ01 hole. The Mohr circles of boreholes LX, ZKJ01, LR1, and CK3 on the western side of the fault zone closely approach the failure threshold for μ=1.0, implying varying levels of fault activity on the eastern side. Overall, the risk of fault slip is higher on the western side from Gongga to Langxian, while it is relatively lower on the eastern side from Linzhi, showcasing the complexity and inhomogeneity of the regional tectonic stress field to some extent.

5 Discussion

Seismic activity is closely linked to fault motion, and the stress field at the fault location serves as a crucial indicator for assessing or forecasting fault motion trends[67–68]. Owing to constraints in deep exploration technology and financial resources, the majority of in situ stress data measurements remain focused on the surface layer of the crust. Nevertheless, the theory of Earth system science posits that the Earth is a complex system, and tectonic movements in the deep crust will inevitably impact the surface layer of the crust. The actual data proved that the accumulation and release of tectonic stresses deep at the seismic source before and after the earthquake were also reflected in the crustal surface layer and the peripheral areas of the seismic source. For example, before and after the Kunlun Mountain M_S8.1 earthquake (November 14, 2001, at a depth of 10 km[69]), a piezomagnetic stress relief method was implemented in Xidatan, Golmud[17], with a maximum depth of 14.0–18.0 m. The maximum horizontal principal stresses of the two measurement holes before the earthquake were 12.9 MPa and 6.8 MPa, and similar stresses were recorded near the measurement holes post-earthquake. Subsequent to the earthquake, the maximum horizontal principal stresses near the boreholes reduced to 3.5 MPa and 2.2 MPa at the same depth, and the orientations of the maximum horizontal principal stresses at the two boreholes experienced significant deflection pre- and post-earthquake. In borehole No.2, the orientation of the maximum horizontal principal stress shifted from N58°E before the earthquake to N8°W after the earthquake. In addition, the crustal stresses at shallow depths (measurement depths less than 13 km) exhibited notable deflection pre- and post-M_S7.0 earthquake in Lushan, which occurred at a depth of 13 km. The same phenomenon of horizontal principal stress change is also present in shallow in-situ stress measurement data (measurement depth less than 400 m) [70]. These observations indicate that while direct observation of the in-situ stress state in the deep part of the earthquake source is challenging with current technical limitations, analyzing the in-situ stress state in the surface layer of the crust using extensive measured data remains valuable for investigating and understanding the activity of deep faults.

Table 2 In situ stress measurement along Yarlung Zangbo River canyon from Rikaze to Linzhi

Measurement point	Measurement segment number	Depth of measurement segment /m	Principal stress/ MPa			Pore pressure P_0/MPa	Fracture orientation /(°)	Note
			S_H	S_h	S_v			
CK3	1	133.00	9.51	5.75	3.60	0.90	Fail to obtain fracture orientation due to imprinter malfunction	Cao et al.[43] (Data from the western side)
	2	170.00	13.01	6.80	4.60	1.27		
	3	241.00	18.12	10.90	6.50	1.98		
	4	261.00	8.82	6.01	7.00	2.18		
	5	283.00	17.53	10.31	7.60	2.40		
	6	296.00	13.59	9.08	8.00	2.53		
LR1	1	64.04	4.81	3.64	1.73	0.47	—	Jiao et al.[42] (Data from the western side)
	2	77.50	6.95	4.77	2.09	0.60	N38°E	
	3	95.25	5.62	4.45	2.57	0.78	—	
	4	103.55	9.21	7.04	2.80	0.86	N33°E	
	5	112.68	7.30	5.13	3.04	0.95	—	
	6	121.27	8.89	5.21	3.28	1.04	—	
	7	125.47	10.33	7.05	3.39	1.08	N30°E	
LR2	1	40.28	2.01	1.50	1.09	0.00	—	Jiao et al.[42] (Data from the western side)
	2	58.45	2.27	2.08	1.58	0.00	—	
	3	71.04	2.42	1.61	1.92	0.00	—	
	4	96.13	4.12	2.76	2.60	0.00	N42°E	
	5	104.20	5.58	3.54	2.81	0.00	N43°E	
LX	1	150.40	13.20	7.98	3.99	1.50	N3°W	Meng et al.[39] (Data from the western side)
	2	183.86	15.16	9.03	4.87	1.84	N4°E	
	3	222.98	18.66	11.15	5.91	2.23	—	
	4	242.90	20.52	12.69	6.44	2.43	—	
	5	250.90	22.29	13.52	6.65	2.51	—	
ND	1	117.00	5.45	3.42	3.10	0.87	—	Meng et al.[39] (Data from the western side)
	2	131.20	6.37	4.20	3.48	1.01	—	
	3	146.50	9.25	6.00	3.88	1.17	—	
	4	178.30	5.22	3.76	4.72	1.48	—	
	5	190.80	6.83	4.48	5.06	1.61	—	
	6	216.80	11.85	6.94	5.75	1.87	N12°E	
	7	226.30	14.90	8.67	6.00	1.96		
	8	247.23	14.02	8.50	6.55	2.17	N28°E	
	9	273.30	12.97	7.83	7.24	2.43	N14°W	
	10	295.80	9.53	6.15	7.84	2.66	N28°E	
	11	370.00	23.40	14.52	9.81	3.40	—	
	12	396.30	30.30	16.69	10.50	3.66	—	
	13	463.70	28.84	16.25	12.29	4.34	—	
ZM	1	205.85	9.41	5.61	5.34	1.41	N9°W	Wang et al.[40] (Data from the western side)
	2	297.7	10.58	7.7	7.72	2.33	—	
	3	392.1	11.36	8.61	10.18	3.27	N6°W	
	4	477.2	12.58	9.7	12.39	4.12	—	
	5	582.85	17.72	13.1	15.13	5.18	N7°E	
GLL	1	40.24	2.50	1.40	1.09	0.10	—	Xie et al.[41] (Data from the eastern side)
	2	44.95	2.60	1.70	1.21	0.10	N65°E	
	3	58.31	3.30	2.00	1.57	0.20	—	
	4	67.25	3.60	2.30	1.82	0.30	—	
	5	82.36	3.70	3.00	2.22	0.50	—	
	6	90.10	4.50	3.20	2.43	0.60	N75°E	
LZ	1	102.50	3.74	2.74	2.72	0.77	—	Meng et al.[39] (Data from the eastern side)
	2	115.00	6.68	4.18	3.05	0.89	—	
	3	125.50	6.85	4.26	3.33	1.00	N6°W	
	4	137.50	4.73	3.22	3.64	1.12	—	
	5	149.20	5.12	3.66	3.95	1.23	—	
	6	156.00	4.01	3.04	4.13	1.30	—	
	7	165.00	3.92	3.11	4.37	1.39	—	
	8	182.30	8.32	5.63	4.83	1.56	N31°E	
	9	188.40	8.54	6.28	4.99	1.62	—	
	10	196.40	5.24	3.88	5.20	1.70	—	
	11	208.00	8.09	6.44	5.51	1.82	N21°E	
	12	239.53	7.39	4.99	6.35	2.14	—	
	13	250.20	12.62	7.88	6.63	2.24	—	
	14	288.00	9.45	6.15	7.63	2.62	—	
	15	295.93	7.22	5.04	7.84	2.70	—	

The mechanism of deep crustal tectonic movement affecting the stress state on the crustal surface remains a challenging issue in geodynamics. Our knowledge about the tectonic morphology of deep faults, the physical and mechanical properties of rocks, and the earthquake processes triggered by fault activity is still insufficient. In situ stress, characterized by strong dispersion, is influenced not only by tectonic movement but also by factors like stratigraphic lithology, discontinuous tectonic surfaces, and topography. There are still limitations in using in situ stress data to assess or predict the activity state of deep faults. Exploring different sections of the eastern Yarlung Zangbo River fault zone using measured in situ stress data is a valuable endeavor, offering insights for related research. However, further improvements are needed to enhance our understanding of the correlation mechanism between in situ stress and tectonic activity in future studies.

6 Conclusion

The in situ stress was measured through field tests conducted near the Yarlung Zangbo River fault zone in the southern Qinghai–Xizang Plateau using the hydraulic fracturing method. This method initially provides insight into the current state of in situ stress in the project area. The analysis of the gathered in situ stress data and application of the Mohr-Coulomb friction-slip criterion help explore the fault activity in the eastern segment of the Yarlung Zangbo River fault zone.

(1) The current tectonic stress in the project area is prominently manifested within the depth range of 122.75–418.75 m of the ZKJ01 borehole, primarily characterized by horizontal principal stress. The maximum horizontal principal stress varies from 6.07 MPa to 37.62 MPa, while the minimum horizontal principal stress ranges between 3.13 MPa and 20.33 MPa.

(2) In the ZKJ01 hole, the relationship between the principal stresses is $S_H > S_h > S_v$. This stress structure promotes development and activity of the reverse thrust fault.

(3) The maximum horizontal principal stresses measured in the ZKJ01 borehole range from N 2 to 26 ℃, with a predominant orientation towards NNE. This alignment aligns well with the regional tectonic stress field and the direction of crustal displacement vector.

(4) The majority of the data obtained from the ZKJ01 borehole intersect with the strength envelope for μ = 0.6. Additionally, the Mohr stress circle at the deep measurement point approaches the upper limit, suggesting a potential sliding risk of the fault near the measurement location.

(5) Based on the in situ stress data measurements, the likelihood of fault slip is greater in the eastern segment of the Yarlung Zangbo River fault zone. There is a higher risk of fault slip in the western section of the fault zone spanning from Gongga to Langxian, while the risk is lower in the eastern section of the fault zone near Linzhi.

References

[1] CHEN Qun-ce, AN Qi-mei, SUN Dong-sheng, et al. Current in-situ stress state of Shanxi Basin and analysis of earthquake risk[J]. Acta Geoscientica Sinica, 2010, 31(4): 541−548.

[2] CHEN Qun-ce, SUN Dong-sheng, CUI Jian-jun, et al. Hydraulic fracturing stress measurements in Xuefengshan deep borehole and its significance[J]. Journal of Geomechanics, 2019, 25(5): 853−865.

[3] WANG Cheng-hu, GAO Gui-yun, WANG Hong, et al. Integrated determination of principal stress and tensile strength of rock based on the laboratory and field hydraulic fracturing tests[J]. Journal of Geomechanics, 2020, 26(2): 167−174.

[4] WANG Cheng-hu, SONG Cheng-ke, GUO Qi-liang, et al. Stress build-up in the shallow crust before the Lushan earthquake based on the in-situ stress measurements[J]. Chinese Journal of Geophysics, 2014, 57(1): 102−114.

[5] JIN Jie-fang, ZHANG Ya-chen, LIU Kang, et al. Effect of gradient stress on stress wave propagation characteristics of red sandstone[J]. Rock and Soil Mechanics, 2023, 44(4): 952−964.

[6] QIAN Qi-hu. Challenges faced by underground projects construction safety and countermeasures[J]. Chinese Journal of Rock Mechanics and Engineering, 2012, 31(10): 1945−1956.

[7] HE Man-chao, SUI Qi-ru, LI Meng-nan, et al. Compensation excavation method control for large deformation disaster of mountain soft rock tunnel[J]. International Journal of Mining Science and Technology, 2022, 32:951−963.

[8] PENG Jian-bing, CUI Peng, ZHUANG Jian-qi. Challenges to engineering geology of Sichuan-Tibet Railway[J]. Chinese Journal of Rock Mechanics and Engineering, 2020, 39(12): 2377−2389.

[9] GU Jia-cheng, GAO Gui-yun, ZHOU Hao, et al. In-situ stress state and engineering effect in Shangrila-Bangda Section of Yunnan-Tibet Railway[J]. Journal of Engineering Geology, 2022, 30(1): 254−264.

[10] REN Yang, WANG Dong, LI Tian-bin, et al. In-situ geostress characteristics and engineering effect in Ya’an-Xinduqiao section of Sichuan-Tibet Railway[J]. Chinese Journal of Rock Mechanics and Engineering, 2021, 40(1): 65−76.

[11] GUO Ling-dong, FU Guang-yu, SHE Ya-wen, et al. Lithospheric isostasy and risk of reservoir induced

earthquakes along the Yarlung Zangbo River between Sangri and Medog[J]. Chinese Journal of Geophysics, 2021, 64(9): 3220−3231.

[12] YANG Shu-xin, YAO Rui, CUI Xiao-feng, et al. Analysis of the characteristics of measured stress in Chinese mainland and its active blocks and north-south seismic belt[J]. Chinese Journal of Geophysics, 2012, 55(12): 4207−4217.

[13] YAO Rui, YANG Shu-xin, XIE Fu-ren, et al. Analysis on magnitude characteristics of the shallow crustal tectonic stresses field in Qinghai-tibet plateau and its adjacent region based on in-situ stress data[J]. Chinese Journal of Geophysics, 2017, 60(6): 2147−2158.

[14] LIAO Chun-ting, WU Man-lu, ZHANG Chun-shan, et al. Recent ground stress measurement of the Kunlun Mountains and Yangbajing Area in Qinghai-Tibet Plateau and its engineering significance[J]. Acta Geoscientica Sinica, 2002, 23(4): 353−357.

[15] WU Man-lu, ZHANG Chun-shan, LIAO Chun-ting, et al. The recent state of stress in the central Qinghai-Tibet Plateau according to in-situ stress measurements[J]. Chinese Journal of Geophysics, 2005, 48(2): 327−332.

[16] ZHANG Chun-shan, WU Man-lu, LIAO Chun-ting, et al. The result of current stress measurements and stress state analysis in the region of Yangbajing-Kangmar in Tibet[J]. Chinese Journal of Geophysics, 2007, 50(2): 517−522.

[17] LIAO C T, ZHANG C S, WU M L, et al. Stress change near the Kunlun fault before and after the Ms 8.1 Kunlun Earthquake[J]. Geophysical Research Letters, 2003, 30(20): 31−34

[18] YAN Jian, HE Chuan, WANG Bo, et al. Inoculation and characters of rockbursts in extra-long and deep-lying tunnels located on Yarlung Zangbo Suture[J]. Chinese Journal of Rock Mechanics and Engineering, 2019, 38(4): 769−781.

[19] WEI Guo-jun. Main geological problems of Lhasa-Xigaze Railway in Brahmaputra Canyon Area and counter measures[J]. Journal of Railway Engineering Society, 2013, 30(4): 21−25, 50.

[20] PAN Gui-tang, LI Xing-zhen, WANG Li-quan, et al. Preliminary division of tectonic units of Qinghai-Tibet Plateau and its adjacent regions[J]. Geological Bulletin of China, 2002, 21(11): 701−707.

[21] LIU Fu-cai, PAN Jia-wei, LI Hai-bing, et al. Characteristics of quaternary activities along Riganpei Co fault and seismogenic structure of the July 23, 2020, M_w6.4 Nima Earthquake, Central Tibet[J]. Acta Geoscientica Sinica, 2022, 43(2): 173−188.

[22] YIN A, HARRISON T M. Geologic evolution of the Himalayan-Tibetan Orogen[J]. Annual Review of Earth and Planetary Sciences, 2000, 28(1): 211−280.

[23] XU Zhi-qin, YANG Jing-sui, LI Hai-bing, et al. On the tectonics of the Indian-Asia collision[J]. Acta Geologica Sinica, 2011, 85(1): 1−33.

[24] LAO Xiong. On the formation of Yarlung Zangbo River Fault Zone[J]. Journal of Geomechanics, 1995, 1(1): 53−59.

[25] PENG Xiao-long, WANG Dao-yong. Active structural characteristics and activity analysis of Yarlung Zangbo river fault zone[J]. Journal of Yangtze University (Natural Science Edition), 2013, 10(26): 41−44.

[26] BIAN Shuang, YU Zhi-quan, GONG Jun-feng, et al. Spatiotemporal distribution and geodynamic mechanism of the nearly NS-trending rifts in the Tibetan Plateau[J]. Journal of Geomechanics, 2021, 27(2): 178−194.

[27] ZHANG Pei-zhen, WANG Min, GAN Wei-jun, et al. Slip rates along major active faults from GPS measurements and constraints on contemporary continental tectonics[J]. Earth Science Frontiers, 2003, 10(Suppl.1): 81−92.

[28] ZHANG Yong-shuan, HU Dao-gong, WU Zhong-hai, et al. Research on the crustal stability and key engineering geological problems along the Yunnan-Tibet railway[M], Beijing: Geological Publishing House, 2009.

[29] BAI Ling, SONG Bo-wen, LI Guo-hui, et al. Seismic activity in the Himalayan orogenic belt and its related geohazards[J]. Advances in Earth Science, 2019, 34(6): 629−639.

[30] BAI Ling, LI Guo-hui, KHAN N G, et al. Focal depths and mechanisms of shallow earthquakes in the Himalayan–Tibetan region[J]. Gondwana Research, 2017, 41: 390−399.

[31] BARUAH SANTANU, BARUAH SAURABH, KAYAL J R. State of tectonic stress in northeast India and adjoining south Asia region: an appraisal[J]. Bulletin of the Seismological Society of America, 2013, 103(2): 894−910.

[32] PRASATH R A, BANSAL B K, VERMA M. Stress distribution in the western India-Eurasia collision zone, its kinematics and seismotectonic implications[J]. Journal of Asian Earth Sciences, 2022, 230: 1−15.

[33] CHEN Ping-guang, HE Xiao-hui, XU Shu-feng, et al. Earthquake relocation and regional stress field around the eastern Himalayan syntaxis[J]. Reviews of Geophysics and Planetary Physics, 2023, 54(6): 667−683.

[34] WU Xiao-long, XIANG Yang, TANG Fu-quan. Study on current crustal deformation of the Himalayan Tectonic Zone by GPS strain-rate estimation and focal mechanism stress inversion[J]. Chinese Journal of Geophysics, 2022, 63(8): 2924−2939.

[35] ZHANG Chen, JI Ling-yun, ZHU Liang-yu, et al. Analysis of the crustal deformation of the Himalayan syntaxis arears based on the earthquake focal stress and GPS strain[J]. Journal of Seismological Research, 2022,

45(4): 526−534.

[36] SUN Yu-jun, GUO Chang-bao, WU Zhong-hai, et al. Numerical study of the crustal stress, strain rate and fault activity in the Eastern Tibetan Plateau[J]. Acta Geoscientica Sinica, 2017, 38(3): 385−392.

[37] PANG Yan-jin, ZHANG Huai, SHI Yao-lin, et al. Plume-induced rifting of thickened crust: 2D numerical model and implications for N–S rifts in Southern Tibet[J]. Geophysical Research Letters, 2022, 49(23): 1−10.

[38] ZHANG Zhen, ZHENG Qun-fan, ZHANG Huai, et al. Late mesozoic multi-plate convergence in East Asia: Insights from 3-D global mantle flow models[J]. Tectonophysics, 2022, 845: 229636.

[39] MENG Wen, GUO Chang-bao, ZHANG Chong-yuan, et al. In situ stress measurements and implications in the Lhasa terrane, Tibetan Plateau[J]. Chinese Journal of Geophysics , 2017, 60(6): 2159−2171.

[40] WANG Qing-wu, JU Neng-pan, DU Ling-li, et al. Three-dimensional inverse analysis of geostress field in the Sangri-Jiacha Section of Lasa-Linzhi Railway[J]. Rock and Soil Mechanics, 2018, 39(4): 1450−1462.

[41] XIE Ping, JIN Hua, CAO Zhong-quan, et al. Analysis on stress field in eastern Xizang[J]. Plateau Earthquake Research, 2007, 19(3): 35−40.

[42] JIAO Guo-feng. Analysis on crustal stress distribution characteristics in canyon areas along Lhasa-Rikaze railway line[J]. Shanxi Architecture, 2008, 34(5): 169−170.

[43] CAO Zhong-quan, XIE Ping, JIN Hua, et al. Variety characteristics of the crustal stress field near the Brahmaputra fault zone[J]. Progress in Geophysics, 2003, 18(1): 167−172.

[44] China Earthquake Administration. DB/T 14 — 2018 Specification of hydraulic fracturing and overcoring method for in-situ stress measurement [S]. Beijing: China Quality and Standards Publishing & Media Co. Ltd., 2018.

[45] HAIMSON B C, CORNET F H. ISRM suggested methods for rock stress estimation-part 3: hydraulic fracturing (HF) and/or hydraulic testing of pre-existing fractures (HTPF)[J]. International Journal of Rock Mechanics and Mining Sciences, 2003, 40(7−8): 1011−1020.

[46] ITO T, HAYASHI A. Analysis of crack reopening behavior for hydrofrac stress measurement[J]. International Journal of Rock Mechanics and Mining Sciences & Geomechanics Abstracts, 1993, 30(7): 1235−1240.

[47] HAIMSON B C, LEE M Y, FEKNOUS N, et al. Stress measurement at the site of the SM3 hydroelectric scheme near sept Iles, Quebec[J]. International Journal of Rock Mechanics and Mining Sciences & Geomechanics Abstracts, 1996, 33(5): 487−497.

[48] ZHANG Chong-yuan, CHEN Qun-ce, QIN Xiang-hui, et al. In-situ stress and fracture characterization of a candidate repository for spent nuclear fuel in Gansu, Northwestern China[J]. Engineering Geology, 2017, 231: 218−229.

[49] BROKER Kai, MA Xiao-dong. Estimating the least principal stress in a granitic rock mass systematic mini-frac tests and elaborated pressure transient analysis[J]. Rock Mechanics and Rock Engineering, 2022, 55: 1931−1954.

[50] HAIMSON B C, LEE M Y, SONG I. Shallow hydraulic fracturing measurements in Korea support tectonic and seismic indicator of reginal stress[J]. International Journal of Rock Mechanics and Mining Sciences, 2003, 40(7−8): 1243−1256.

[51] KIRSCH C. Die theorie der elastizitat und die bedurfnisse der festigkeitslehre[J]. Zeitschrift Des Vereines Deutscher Ingenieure 1898, 42: 797−807.

[52] CHOU Wan-xi, LI Wei, WEI Shan-bin, et al. Rockmass stress measurement by sleeve fracturing technique and calculation on initial rockmass stresses[J]. Chinese Journal of Rock Mechanics and Engineering, 1996, 15(1): 40−47.

[53] JING Wei, XUE Wei-peng, HAO Peng-wei, et al. Principal and method of sleeve fracturing method in testing in-situ stress[J]. Journal of China Coal Society, 2015, 40(2): 342−346.

[54] HAYASHI K, HAIMSON B C. Characteristics of shut-in curves in hydraulic fracturing stress measurement and determination of in situ minimum compressive stress[J]. Journal of Geophysical Research, 1991, 96(11): 18311−18321.

[55] GRONSETH J M, KRP P R. Instantaneous shut-in pressure and its relationship to the minimum in situ stress, hydraulic fracturing stress measurements[M]. Washington D. C.: National Academy Press, 1983.

[56] FENG Cheng-jun, CHEN Qun-ce, WU Man-lu, et al. Analysis of hydraulic fracturing stress measurement data—discussion of methods frequently used to determine instantaneous shut-in pressure[J]. Rock and Soil Mechanics, 2012, 33(7): 2149−2159.

[57] LIN W R, YEH E C, HUNG J H, et al. Localized rotation of principal stress around faults and fractures determined from borehole breakouts in hole B of the Taiwan Chelungpu-fault Drilling Project (TCDP)[J]. Tectonophysics, 2010, 482(1−4): 82−91.

[58] ZHANG S H, MA X D. How does in situ stress rotate within a fault zone? Insights from explicit modeling of the frictional, fractured rock mass[J]. Journal of Geophysical Research: Solid Earth, 2021, 126(11): 1−23.

[59] ZOBACK M D, ROLLER J C. Magnitude of shear stress on the San Andreas fault: implications of a stress measurement profile at shallow depth[J]. Science, 1979,

206(4417): 445−447.

[60] XIE Fu-ren, CUI Xiao-feng, ZHAO Jian-tao, et al. Regional division of the recent tectonic stress field in China and adjacent areas[J]. Chinese Journal of Geophysics, 2004, 47(4): 654−662.

[61] XIE Fu-ren, CHEN Qun-ce, CUI Xiao-feng, et al. Fundamental database of crustal stress environment in continental China[J]. Progress in Geophysics , 2007, 22(1): 131−136.

[62] XIE Zhou-min, CAI Yong-en, SHOICHI Yoshioka, et al. Exploring the location of large earthquakes using fault stress accumulation－a case study upon M_W9.0 Tohoku-Oki earthquake in Japan[J]. Chinese Journal of Geophysics, 2022, 65(1): 1−11.

[63] ZHANG Hao, SHI Gang, WU Hong, et al. In situ stress measurement in the shallow basement of the Shanghai area and its structural geological significance[J]. Journal of Geomechanics, 2020, 26(4): 583−594.

[64] BYERLEE J D. Friction of rock[J]. Pure and Applied Geophysics, 1978, 116: 615−626.

[65] ZOBACK M D, HICKMAN S. In situ study of the physical mechanisms controlling induced seismicity at Monticello reservoir, south Carolina[J]. Journal of Geophysical Research, 1982, 87(8): 6959−6974.

[66] ZOBACK M D. Reservoir geomechanics[M]. New York: Cambridge University Press, 2007.

[67] MUSKAT M. Use of data on build-up of bottom hole pressure[J]. Transactions of the AIME, 1937, 123(1): 44−48.

[68] MCGRRR A, GAY N C. State of stress in the earth’s crust[J]. Annual Review of Earth and Planetary Sciences, 1978, 6(1): 405−436.

[69] ZHOU Yun-hao, CHEN Zhang-li, MIAO Fa-jun. Source process of the 10 November 2001western Kunlun Mountain M_S 8.1 earthquake[J]. Acta Seismological Sinica, 2004, 26(Suppl.): 9−20.

[70] WU M L, ZHANG C Y, FAN T Y. Stress state of the Baoxing segment of the southwestern Longmenshan fault zone before and after the Ms7.0 Lushan earthquake[J]. Journal of Asian Earth Sciences, 2016, 121: 9−19.